Article

The Changes in Multiscale Solar Wind Fluctuations on the Path from the Sun to Earth

Igor D. Volodin [1], Maria O. Riazantseva [2,*], Liudmila S. Rakhmanova [2], Alexander A. Khokhlachev [2] and Yuri I. Yermolaev [2]

1   Faculty of Mathematics, Computer Science and Physics, University of Innsbruck, 6020 Innsbruck, Austria; igor.volodin@student.uibk.ac.at
2   Space Research Institute of the Russian Academy of Sciences (IKI), Moscow 117997, Russia; rakhlud@gmail.com (L.S.R.); aleks.xaa@yandex.ru (A.A.K.); yermol@iki.rssi.ru (Y.I.Y.)
*   Correspondence: orearm@gmail.com

Abstract: This paper is devoted to the analysis of fluctuations in the solar wind plasma and interplanetary magnetic field parameters observed by Solar Orbiter and WIND spacecraft at different scales ranging from $\sim 10^3$ to 10^7 km. We consider two long data intervals where the distances between the spacecraft are 0.1 and 0.5 AU, respectively, and they are located close to the Sun–Earth line. Transformation of the fluctuation's properties on the way from the Sun to Earth is analyzed for different types of solar wind associated with quasi-stationary and transient solar phenomena. The time series of bulk speed are shown to undergo a slight modification, even for large spacecraft separation, while the time series of the interplanetary magnetic field magnitude and components as well as proton density may be transformed even at a relatively short distance. Though the large-scale solar wind structures propagate the distance up to 0.5 AU without significant change, local structures at smaller scales may be modified. The statistical properties of the fluctuations such as relative standard deviation or probability distribution function and its moments remain nearly unchanged at different distances between the two spacecraft and are likely to depend mostly on the type of the solar wind.

Keywords: solar wind; interplanetary magnetic field; intermittency; multi-spacecraft observations

1. Introduction

The variability of the solar wind (SW) has been a topic of interest in space science research for a long time. A wide range of spatial structures of the SW can be conventionally classified into different scales [1–3]. Large-scale phenomena in the SW are manifestations of the solar corona structures and attract the greatest interest of researchers (see, for examples, [4–7]). They have spatial scales exceeding 10^6 km and are represented by nonstationary structures like interplanetary coronal mass ejections (ICMEs), including EJECTA and magnetic clouds (MCs), as well as compression regions ahead of ICMEs, named SHEATH, and ahead of fast streams, named corotating interaction regions (CIRs). They also include quasi-stationary structures—heliospheres current sheet (HCS), fast streams from the coronal holes (FASTs), and slow streams from the coronal streamers (SLOWs) (in this study, we use classification of the large-scale structures described in [6]). Small-scale structures with scales of thousands of kilometers and under represent processes such as instabilities, waves, and other local phenomena [8]. At the middle scales ($\sim 10^5$–10^6 km), there is variety of magnetohydrodynamic (MHD) structures such as Alfvén waves, flux tubes, etc. [9–11]. Moreover, there are short-term SW phenomena which separate the MHD structures, such as discontinuities of different types, i.e., interplanetary shocks (IS) and reverse shocks (ISa) [12]. For fast-moving phenomena, temporal scales should be taken into account. The SW speed is usually much greater than a spacecraft's speed, and the latter can be neglected (i.e., a spacecraft is assumed to stay motionless in the plasma frame). In this case, according to Taylor's hypothesis [13], we can determine a spatial scale of the flow structures with the

help of single-spacecraft measurements. At the same time, multipoint observations allow us to study the space inhomogeneity and dynamics of the structures.

The majority of research on SW are based on in situ measurements near Earth. As a rule, they use the measurements of spacecraft at Lagrange L1 point (ACE, WIND, DSCOVR), spacecraft with high apogee orbits (IMP-8, Geotail, Interball-1, Spektr-R, and others), or magnetosphere missions at the moments when their orbits lie in the SW (Cluster, Themis/Artemis, MMS). Measurements of the SW on spacecraft with different radial distances (Helios, Voyager etc.) are usually compared statistically, while comparisons of simultaneous measurements are presented rarely. However, multipoint analysis on a large spatial basis is very important. For instance, it helps to specify the propagation vector of a phenomenon and to identify variations within it more carefully. Despite the technical difficulties of such a comparison, a number of authors have performed analyses of SW parameters obtained from several distant spacecraft. For example, Burlaga et al. [14] studied the interplanetary magnetic field (IMF) and plasma parameters during observation of a magnetic cloud, an interplanetary shock before it, and a turbulent Sheath region behind the shock with the help of simultaneous data from Voyager, Helios, and IMP-8 spacecraft. The authors succeeded in estimating the size of the loop in two planes. Also, the authors revealed the extraordinary filament at the rear part of the cloud, with its boundaries keeping their orientation over at least 0.12 AU. However, most of such research is recent due to the increasing number of spacecraft in the heliosphere. Prise et al. [15] traced the propagation of closely observed ICME and CIR events and showed that these phenomena merged together even before they reached Saturn. A detailed study of the ICME expansion on the path from Mercury to Earth is provided in [16]. Good et al. [17] investigated the observation of flux ropes at radially aligned spacecraft (MESSENGER, Venus Express, WIND, STEREO) and showed that they often had very similar features at different spacecraft, while the observed macroscale difference could be explained by various orientation of the flux rope. In [18], the authors succeeded in restoring a global configuration of interacted, but not merged, ICMEs based on measurements of more than five spacecraft. In a recent paper by the same authors [19], the primary identification of ICMEs was performed using images from STEREO-A, and then interplanetary propagation of the events was traced using in situ measurements from Solar Orbiter (SolO), WIND, Bepi-Colombo, Parker Solar Probe (PSP), and STEREO-B. The use of multipoint measurements, including the spacecraft closer to the Sun (SolO and PSP), allowed the authors to more accurately determine the evolution of the ejection shape and its parameters, such as speed, propagation vector, and magnetic field magnitude. The analysis revealed an important role of the interacting magnetic flux ropes in the dynamics of coronal mass ejections and their subsequent impact on the surrounding environment.

Most of the papers have described the multipoint analysis of large-scale structures such as ICME, CIR, and their general features in the heliosphere. However, the SW varies at a wide range of scales due to interactions between different structures and turbulent plasma [20]. Studies of the SW fluctuation properties in different positions in the heliosphere and their dynamics are also relevant, but the number of such studies is not yet large; moreover, most of them are statistical studies. For example, Bruno et al. [21] analyzed the SW fluctuation properties using measurements of the Helios 2 spacecraft. This study focused on features of probability distribution function (PDF) of the SW speed and IMF vector fluctuations in several SW types and at different distances from the Sun. The authors showed that an increase in intermittency with distance from the Sun was observed in fast streams from coronal holes, while PDF in slow streams from coronal streamers did not exhibit any radial dependence of the fluctuation properties. The evolution of turbulence was also studied in [22] on the base of Ulysses and ACE data, and intermittency was shown to grow with the distance. Several radially aligned positions of WIND and MESSENGER were used in [23], and the results demonstrated the evolution of turbulent spectra properties with distance. The detailed review of the investigation of the SW turbulence evolution in the inner heliosphere is presented in [24].

The launch of the SolO, PSP, and BepiColombo spacecraft provided an opportunity for investigation of the evolution of the turbulent SW fluctuations in the inner heliosphere due to the high time resolution of the measurements and the suitable configuration of the orbits for multipoint observations. For example, the evolution of IMF fluctuation properties such as scaling, high-order statistics, and multifractal features was analyzed in [25] with the help of PSP and BepiColombo, which were located radially at different heliocentric distances. It was shown that the role of dissipation mechanisms changed with the distance from the Sun. Based on the first radial alignment of the PSP and SolO spacecraft, Telloni et al. [26] studied the evolution of the SW turbulence properties in the heliosphere and showed that, near the Sun, highly Alfvenic less-developed turbulence was observed, whereas the turbulence became fully developed and intermittent closer to Earth. Sioulas et al. [27] investigated the radial evolution of the anisotropy properties of the SW turbulence.

The aforementioned studies demonstrate the effectiveness and relevance of multi-spacecraft analysis for exploration of the SW evolution in the heliosphere. However, despite the abundance of experimental data at the present moment, such a multi-point approach is still poorly developed due to the difficulties of instrument intercalibration and inconsistency of spacecraft operation. At the same time, the relevance of this topic is beyond doubt, because the dynamics and features of different types of the SW structures are crucial for predicting the impact of these structures on the Earth's magnetosphere, i.e., in a framework of space weather. The existing SW models can predict the behavior of plasma and magnetic field parameters mostly in terms of large-scale dynamics. On the other hand, the phenomena observed at medium and small scales can significantly reduce the quality of prediction. Thus, studies on the dynamics of smaller-scale structures are of particular interest for the development of SW models.

The present study adopts multipoint analysis for a comprehensive comparison of simultaneous observations on two spacecraft (SolO and WIND) located along the Sun–Earth line at different heliocentric distances. The selection of long intervals allowed us to analyze the evolution of different large-scale structures. At the same time, using the maximum available temporal resolution of measurements (down to fraction of second) made it possible to analyze the evolution of fluctuation properties at a wide range of scales.

2. Data and Methods

2.1. Data Source

This study analyzes measurements on the WIND and SolO spacecraft to observe the SW structures at different heliospheric distances. The WIND spacecraft (in operation since November 1994) has an orbit near the L1 libration point. The IMF study on this spacecraft was carried out using the MFI magnetometer [28], which has a temporal resolution of ~0.1 s. The study also uses data from the 3DP analyzer [29], which provides data on various SW plasma parameters every 3 s. Since the sensors of the 3DP plasma instrument have degraded to some extent during the mission, it is necessary to verify and correct the measured values of plasma parameters. To solve this problem, the data from another plasma instrument, SWE [30], are used as a reference for comparison and adjustment purposes. The SWE instrument includes Faraday cup sensors, which are stable over time and give reliable measurements of plasma parameters for about 30 years. The time resolution of the SWE measurements is ~1.5 min, which is not suitable for analyzing small-scale structures. For this reason, in the present study, the SWE measurements are used only for verification of the 3DP measurements. The SolO spacecraft has been in operation since February 2020, and its main task is to explore the plasma and magnetic field parameters of the solar atmosphere in detail at short heliocentric distances simultaneously with observations of the solar disk and corona. It follows a complex orbit around the Sun at distances ranging from 0.28 to 1.4 AU. We use data from the SolO MAG magnetometer [31], which provides continuous, highly accurate magnetic field vector measurements with a time resolution of 0.125 s. For the analysis of plasma parameters, data from the SWA instrument [32] with a time resolution

of 4 s are used. This study includes a comparison of long-term time series of plasma and IMF parameters measured simultaneously on two spacecraft.

The following set of parameters is analyzed: bulk speed, proton density, temperature and magnitude, and components of the IMF. The CDAWeb database (https://cdaweb.gsfc.nasa.gov/ (accessed on 17 May 2023)) is used as a source of data on spacecraft coordinates, SW plasma, and IMF parameters. The time series under consideration are tied to the types of the large-scale SW phenomena. Different SW types are identified using the IKI catalog of large-scale phenomena (http://www.iki.rssi.ru/pub/omni/catalog/ (accessed on 17 April 2023)) [6]. The catalog contains information from 1976 to 2022 on different types of SW: ICME (we highlight EJECTA in the figures below in blue color and MC in red), HCS (orange), SLOW (grey), FAST (brown), CIR (lime-green), and SHEATH (black). The IKI catalog provides 1 h data, so the boundaries of different SW types are not displayed accurately for time series with better time resolutions. Therefore, we use the catalog information as the first approach and further refine the boundaries for each interval if needed.

2.2. Selection of Events near the Sun–Earth Line

High-speed flows from coronal holes and transient flows of the ICMEs are the primary objects of our study because such phenomena are known to be geoeffective and to propagate nearly radially from the Sun [33]. To select the events of interest, we analyzed the orbits of the spacecraft in the HEEQ coordinate system [34], identifying the time intervals when the SolO located in the ecliptic plane approached the Sun–Earth line. The initial criterion of approaching was a distance from the spacecraft to the Sun–Earth line (see Equation (1)) of $\sim 10^6$ km.

$$R_{SolO\_SE} = R_{SolO\_S} \times |\sin(\phi_{SolO})| \tag{1}$$

where R_{SolO_SE} and R_{SolO_S} are the distances from the SolO spacecraft to the Sun–Earth line and to the Sun and ϕ_{SolO} is the longitude of the spacecraft in the HEEQ coordinate system.

In this way, we selected two long intervals during which the SolO spacecraft was located in the vicinity of the Sun–Earth line, but at different distances from the Earth. When the SolO was closer to Earth, it moved for a long time near the Sun–Earth line. In the case when SolO was closer to the Sun, it crossed the region of interest very quickly. We selected intervals so that their durations became similar, and both intervals included a diverse set of large-scale structures.

The first event (total duration: ~9 days) was observed from 5 November 2021 13:54:00 UT to 14 November 2021 13:25:00 UT (time was given after shifting to the WIND time series), when the SolO was relatively close to the Earth's orbit, with a distance of ~0.1 AU upstream from the WIND spacecraft (see the left panel in Figure 1). During the second event, the SolO was about 0.5 AU upstream from WIND (see the right panel in Figure 1). The event spanned from 2 March 2022 21:05:00 UT to 12 March 2022 7:11:00 UT (total duration: ~9.5 days).

2.3. Data Tracing and Correlation Analysis

The next step was to trace the data measured at SolO to the orbit of WIND. A preliminary time shift between time series was calculated with the help of Equation (2) based on the spacecraft locations and the SW bulk speed. The numerator represents the difference between the X-coordinates of the SolO and WIND spacecraft in the HEEQ coordinates, and the denominator represents the mean bulk speed.

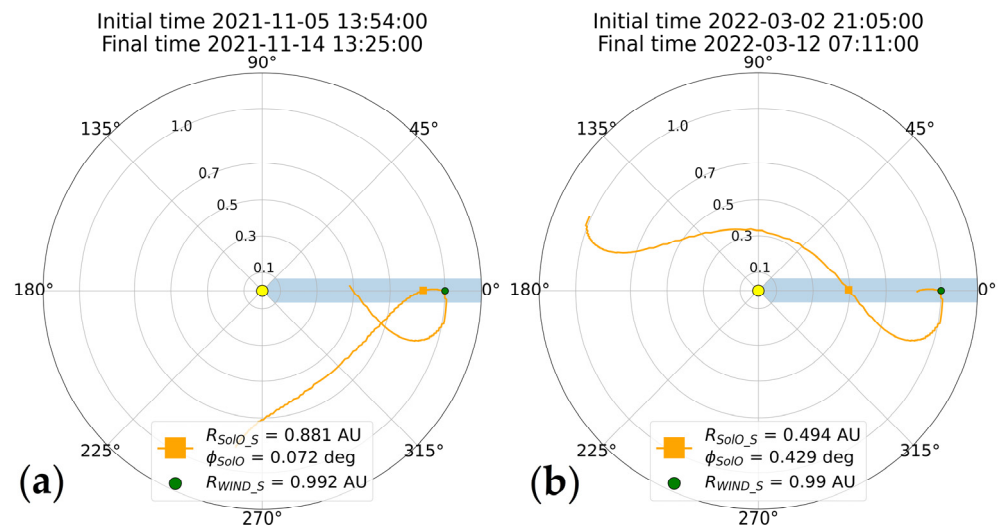$$\Delta t = \frac{X_{WIND\_S} - X_{SolO\_S}}{\langle V \rangle} \tag{2}$$

Figure 1. Trajectory and coordinates of SolO spacecraft (orange square) and WIND (green circle) in HEEQ coordinates for two analyzed cases. The distances between spacecraft are equal to 0.1 AU for panel (**a**) and 0.5 AU for panel (**b**), respectively.

The time shift given by the Equation (2) is rather imprecise, since it does not reflect the orientation or motion of different structures and their boundaries with different velocities, nor possible changes in velocity as the plasma propagates in the heliosphere. The generally accepted MVA method takes into account not only the bulk speed, but also the inclination of the fronts of various SW structures [35]. However, this method is more complicated and does not always provide correct results, as variations in the velocities of small-scale structures, possible changes in flow direction, and flow variability are not taken into account. In this paper, we use correlation analysis to clarify the time shift between the pair of spacecraft. This method is effective for estimating corrections to the SW propagation time in complicated cases (see, for example, [36]). Below, we consider the scheme for determining the time shift used in this study. The example of tracing proton bulk speed and temperature time series with the help of the preliminary time shift is presented in Figure 2a for the second event (the distance between SolO and WIND is 0.5 AU). Although the average correlation coefficient is rather high (0.68 for bulk speed time series and 0.51 for proton temperature time series), local discrepancies and clear difference in time shifts for different structures can be seen. To simplify the time series comparison and time shift clarification, the long interval was divided into three parts according to large-scale structures moving with different bulk speeds. For the presented example, the interval was divided into three sections: the 5th 0:09:58–10th 2:04:49–11th 12:04:49–14th 10:15:58 of March 2022, with mean speeds of 449, 360, and 407 km/s for WIND and 437, 358, and 375 km/s for SolO, respectively. Thus, according to Figure 2a, during the first selected subinterval, both spacecraft observed substantial increases in speed and temperature values due to the registration of a fast stream from a coronal hole and further decreases in these parameters.

The correlation coefficients for bulk speed and temperature time series for this subinterval were equal to 0.88 and 0.82, respectively. The values of parameters at WIND remained stable during the second subinterval, while substantial large-scale changes were observed by SolO. This difference led to low correlation coefficients for this interval (0.28 for bulk speed and 0.05 for temperature). For the third subinterval, as shown in Figure 2a, both time series exhibited abrupt increases in both speed and temperature at the end, but the correlation coefficients were equal to 0.01 and 0.06, respectively. The low correlation was caused by an incorrectly determined time shift between the data series.
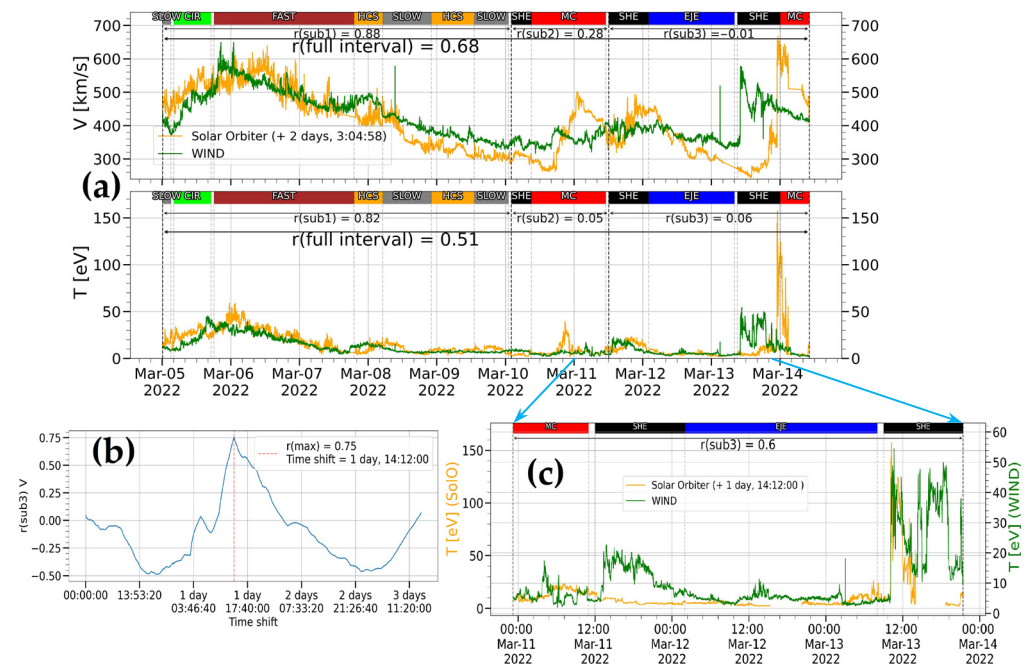
Figure 2. (**a**) Comparison of proton bulk speed (top panel) and proton temperature (bottom panel) time series at the SolO and WIND with preliminary time shift (2nd event). Correlation coefficients for full interval (r(full interval)) and for subintervals (r(sub1), r(sub2), r(sub3)) are shown in the chart. The color bar at the top of the chart shows the periods of different large-scale SW structures. (**b**) Dependence of the correlation coefficient between bulk speed time series measured at the SolO and WIND on the time shift between them. (**c**) Comparison of proton temperature time series at the SolO and WIND for the third subinterval with the time shift estimated by the correlation analysis. Arrows show that the interval on panel (**c**) is a part from interval on panel (**a**).

In the method based on correlations, the value of the correlation coefficient is considered as a function of a time shift R(dt) between two data series of bulk speed (see, for example, Figure 2b). The range of time shifts considered for the calculation of the correlation coefficient is determined from Equation (2) for the minimum SW speed and for the locations of the spacecraft at the start and at the end of the interval. When time resolutions for the same quantities measured on different spacecraft do not match, the data are interpolated to a common time grid. The time shift which corresponds to the maximum value of the correlation coefficient R(dt) is chosen as real propagation time between two spacecraft.

For example, in Figure 2b, the maximum of the correlation function R(dt) is equal to 0.75 and corresponds to a time shift of 1 day, 14 h, and 12 min. The time shift given by Equation (2) is 2 days, 3 h, and ~5 min (see Figure 2a). Thus, according to WIND observations, the interplanetary shock observed during the interval arrived 15 h earlier than expected based on the average bulk speed estimation (404 km/s). The resulting time delay corresponded to a plasma propagation speed of ~600 km/s, which is consistent with the observed shock speed (see upper panel of Figure 2a). Figure 2c demonstrates that adopting this technique makes it possible to increase the correlation coefficient from 0.06 to 0.6 for the temperature time series. Such corrections were used both for the whole considered interval and for subintervals. This method allowed us to increase the correlation for most of the parameters, especially for the case of large separation between the spacecraft. However, we note that the method reflects the best shift along the most pronounced structures (for example, in this case, along the interplanetary shock front) and may not be suitable for other structures observed during the interval that propagate with different bulk speeds. For example, the plasma structure with the temperature increase, observed on the 11th of March at ~13:00–24:00, matched well according to observations on two spacecraft before

correction, but did not match after the correction. Thus, the propagation time of this structure was close to the mean plasma propagation time.

2.4. Intercalibration

As a rule, there was high correlation for all parameters when the spacecraft were located close to each other. Nevertheless, during this period, the difference in the bulk speed and proton density amplitudes between the SWA instrument (SolO) and the 3DP instrument (WIND) data reached values of 30 km/s and 20 cm^{-3}, respectively. At the same time, the difference between the SWA instrument on SolO and the SWE instrument on WIND was about five times smaller. This fact demonstrated the necessity of making a correction for the 3DP plasma data. We used a numerical criterion of approximation quality according to Equation (3) to intercalibrate 3DP and SWE data on the WIND spacecraft. Equation (3) gives a prediction error parameter (residuals). The summing was performed over all n points of the differences in the squares of the approximated points (fit) and the original points with k-indices.

$$\epsilon o = \sum_{k=0}^{n} \left(y_{fitk} - y_k\right)^2 \tag{3}$$

The lowest prediction error occurred when we used a linear approximation with absolute differences between the parameters in the comparison of the interpolated SWE instrument data and the 3DP measurements with increasing coefficients. Moreover, the SWE WIND plasma data were considered as a reference, and corrections were also made for the SWA SolO data using the measurements from when the spacecraft were close to each other. Similarly, we calculated the decreasing coefficients for the SWA SolO data in order to be able to compare values as the distance between the spacecraft increased.

2.5. Statistical Analysis

Properties of statistical distributions were used to compare the parameters' values at different spacecraft. This approach allowed us to identify individual subsets of the observed plasma flows and determine changes in the main statistical parameters, such as the mean, median, standard deviation (STD), standard deviation normalized to the mean value (Norm STD) reflecting the relative level of fluctuations, and standard error of mean (SEM). The SEM took values in thousandths of the corresponded mean values for all selected intervals, which, coupled with the number of measured points (~10^4), made comparisons of the other parameters at different heliocentric distances statistically valid. The analysis of statistical distributions was carried out not only for the selected time intervals as a whole, but also for individual SW types within them (similar to [37]).

2.6. Fluctuation Level Analysis

The present study considered the transformation of local fluctuation levels and their distribution functions with distance and the roles of different types of SW in this process. For this purpose, the standard deviations normalized to the mean value of the observed parameter were calculated in three-hour subintervals with moving windows throughout the whole interval. The step of the windows moving was equal to the half of the subinterval length in order to avoid a loss of information at the subintervals' edges. The resulting time series of local standard deviations (Loc STD) showed the evolution of the fluctuation level with time and indicated differences for various SW structures. To avoid confusion with the Norm STD obtained from the distributions at the whole interval, the Loc STD below is denoted as $\sigma_t(X_t)/\langle X_t \rangle$, where X_t is the time series of the considered parameter during a given 3 h subinterval and $\sigma_t(X_t)$ is the standard deviation of X_t during the subinterval. The example of the Loc STD time series presented in Figure 3 indicates the increase in the fluctuation level in the vicinity of the HCS.
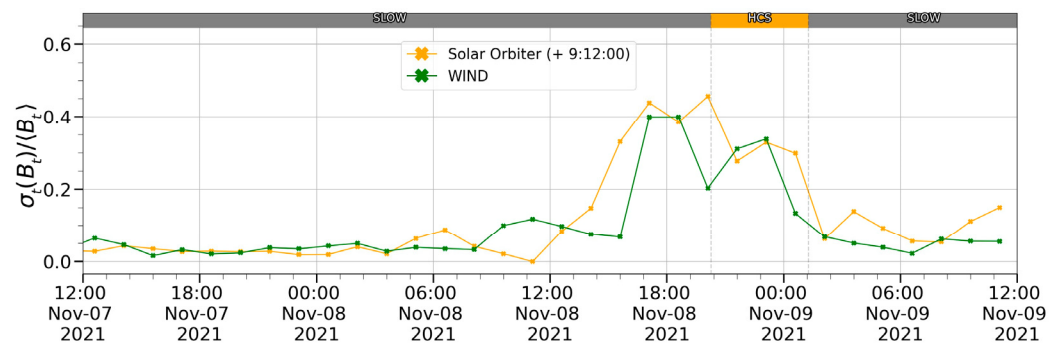
Figure 3. Time evolution of the Loc STD of the IMF magnitude for the SolO and WIND for the first subinterval of the 1st event (12:00 7th–12:00 9th of November 2021).

2.7. Intermittency Analysis

At the second stage of the statistical analysis, we investigated the high-order moments of the fluctuation probability distribution functions (PDFs). The SW turbulent plasma fluctuations are known to be distributed non-uniformly, and the degree of non-uniformity and power of fluctuations may vary in different SW streams [21,38]. This non-uniformity results in deviation of the PDF shape from the normal distribution and in PDFs with heavy tails, which correspond to a high probability of large amplitude fluctuations (see left panel in Figure 4). This kind of PDF is typically observed for small-scale fluctuations, while the PDFs become closer to the normal (Gaussian) distribution with increasing fluctuation scales [39]. This feature of the SW fluctuations is a sign of intermittency [21]. Intermittency can be studied by considering the dependence of the fourth-order moment of the PDF on the scale of fluctuations. First, the time series of the parameter's value variation X are calculated for various time scales τ:

$$\delta X_\tau(t) = X(t + \tau) - X(t) \tag{4}$$

In this study, we used the time scale of fluctuations in a wide range—from the time resolution of the data to tens of hours. The fourth-order moment (named flatness) was determined by Equation (5) (in accordance with [21] and references therein):

$$F_\tau(t) = \frac{\langle |\delta X_\tau(t)|^4 \rangle}{\left(\langle |\delta X_\tau(t)|^2 \rangle \right)^2} \tag{5}$$

where $\delta X_\tau(t)$ is the function defined by Equation (4) for the observed parameter X. The flatness for the normal distribution is equal to 3. A flatness value noticeably higher than 3 indicates the presence of heavy tails and/or a sharp peak in the distribution. In practice, ideal normal distributions are rarely observed for large-scale SW fluctuations, and the flatness can vary in the vicinity of 3. The main signature of the intermittent flow is a decreasing trend of flatness with an increase in the fluctuation scale [21], regardless of the variations in its value, which can be observed [38].

Figure 4a illustrates the PDF of magnetic field magnitude on the time scale of 10 s from SolO and WIND data. The flatness values are 60.1 and 53.7, respectively, and exceed 3 (typical for a normal distribution) substantially. Note that such a similarity in the flatness values can be considered as a match, since the flatness usually varies significantly [38].

Figure 4b illustrates that the 4th moment of the IMF magnitude PDF smoothly decreases as the time scale increases from 4 to 3×10^5 s, which is typical for intermittent SW streams. Moreover, for both spacecraft, the dependences of flatness vs. time scale are similar up to a scale of $\sim 10^4$ s. For larger scales, the flatness values are not stable, which is likely due to the decrease in the statistical significance of the amplitude fluctuations at the corresponding PDFs. The presented example (see Figure 4) indicates the similarity of the

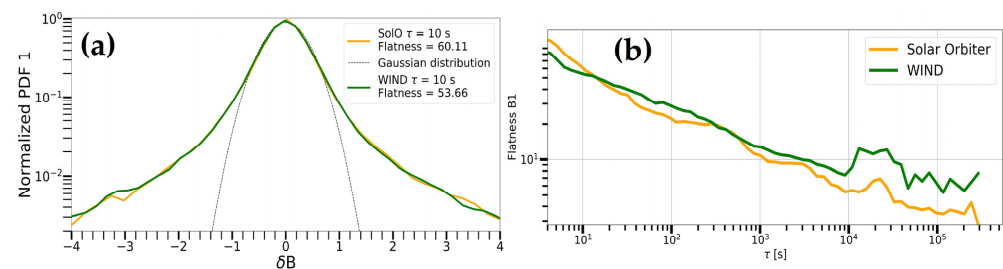statistical properties of magnetic field fluctuations measured at different distances from the Sun.

Figure 4. (**a**) PDF for the IMF magnitude fluctuations on the SolO (orange line) and on the WIND (green line) and its comparison with the Gaussian distribution (black dashed line). (**b**) Dependence of the flatness of the IMF magnitude fluctuations on the time scale of fluctuations in the logarithmic scale for the SolO (orange line) and WIND (green line) (1st event, 1st subinterval).

3. Results

3.1. Correlation Analysis

The correlation coefficient between the same parameters observed on different spacecraft can be interpreted as a measure of the variability of the SW stream on the way from one spacecraft to another. The time series of most of the parameters do not change significantly when the spacecraft are relatively close to each other. Figure 5 shows the time series of the SW plasma and IMF parameters observed on the SolO and WIND during the first selected time interval (the distance between the spacecraft is ~0.1 AU). The best agreement was observed between the proton bulk speeds measured on two spacecraft. In this case, the rough time shift estimate (11 h and 11 min) given by Equation (2) provides a good coincidence of the time series of the bulk speed over the entire event, and the correlation coefficient is 0.97 for the whole interval.

Table 1. Comparison of the time shifts after correction (Δt), correlation coefficients for IMF magnitude (B) and its components (Br, Bt, Bn), proton density (n), bulk speed (V), and temperature (T) for all subintervals at the 1st event (lines 1, 2, and 3) and the 2nd event (lines 4, 5, and 6).

		Δt	B, nT	Br, nT	Bt, nT	Bn, nT	V, km/s	n, cm^{-3}	T, ev
	sub1	9:12	0.46	0.52	0.55	0.23	0.94	0.94	0.84
1st event	sub2	9:06	0.32	0.41	0.05	0.07	0.83	0.7	0.81
	sub3	9:09	0.39	0.01	−0.1	0.43	0.89	0.4	0.86
	sub1	2 days 9:48	0.32	0.02	−0.11	−0.07	0.92	0.43	0.81
2nd event	sub2	2 days 6:08	0.55	−0.27	0.19	0.07	0.3	−0.04	0.07
	sub3	1 day 14:12	0.83	−0.11	−0.52	0.35	0.75	0.38	0.6

The correlation coefficient may vary for shorter subintervals over which different types of structures are observed. The division into subintervals was carried out similarly to the approach described in Section 2, in accordance with the plasma structures allocated: a smooth descent of the bulk speed during the first subinterval, a slight rise and then a decrease during the second one, and a smooth decrease during the third subinterval. At the first subinterval (5 November 2021 13:54:00 UT–9 November 2021 03:50:26 UT), the correlation coefficient for the bulk speed time series reached 0.97; this value was 0.78 for the second subinterval (9 November 2021 03:50:26 UT–11 November 2021 02:50:26 UT) and 0.87 for the third subinterval (11 November 2021 02:50:26 UT–14 November 2021 13:25:00 UT). The correlation coefficients marked in Figure 5 were determined based on the spacecraft separation and the SW speed, because this rough estimation gave good results in this case. Even though there was a difference within the observed structures during the second subinterval, the time series correlated well in general. The temperature values also

showed high similarity with the overall correlation coefficient of 0.83, and was greater than 0.66 on subintervals (Figure 5g). In the case of density, the correlation calculated for the whole interval was rather high: 0.65 (Figure 5f). On the other hand, on the subintervals, it might have been high (0.83, subinterval 2) or low (0.29, subinterval 3). During the first subinterval, the density enhancement (on 7 November 2021) was registered on Wind and was not registered on SolO; however, the subinterval demonstrated high similarity of the density structures. The low correlation for the third subinterval was likely to be caused by discrepancies in the structures observed on 13 November.
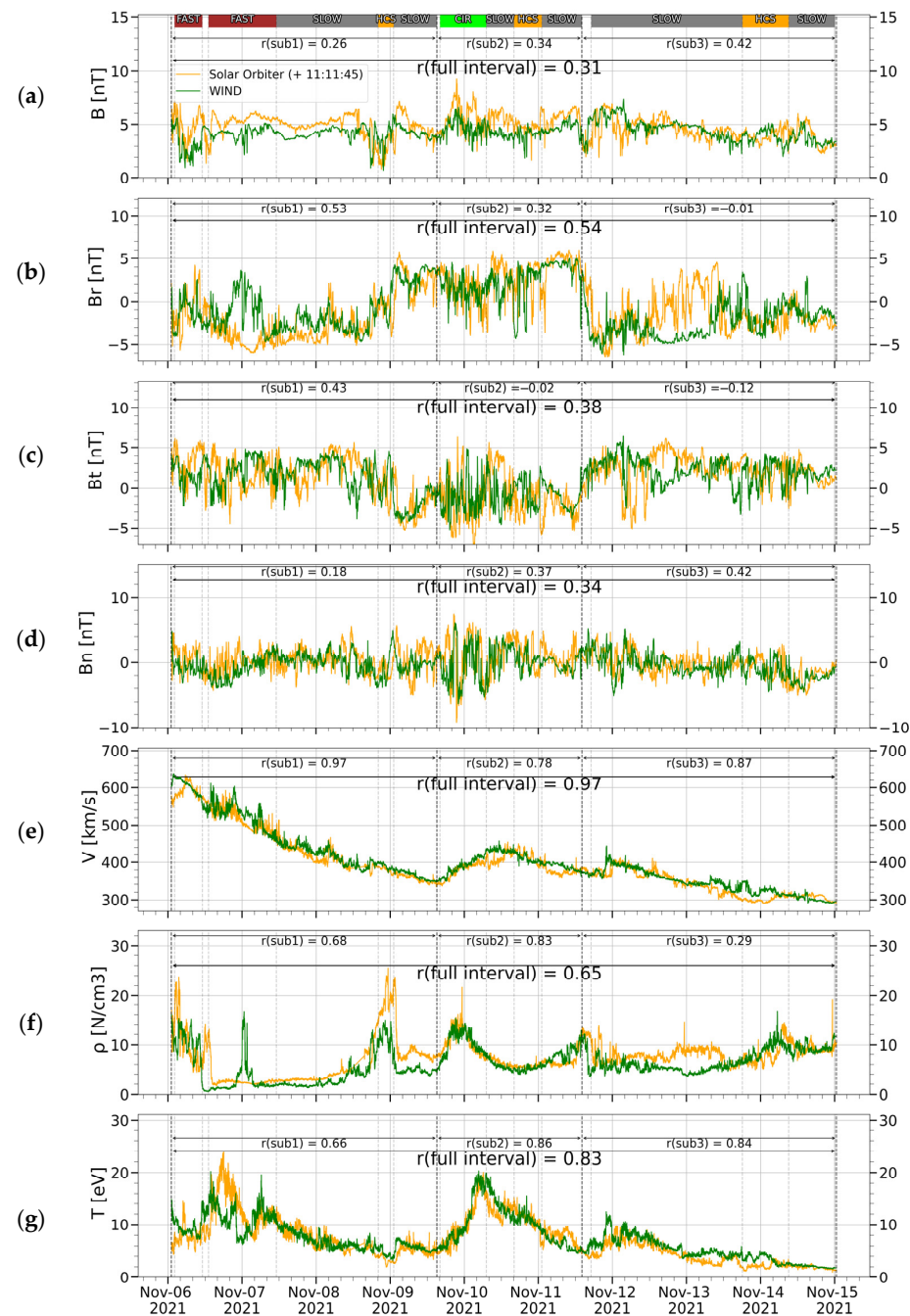

Figure 5. Comparison of the time series of the IMF magnitude (**a**) and its components in the RTN system (**b**–**d**), bulk speed (**e**), proton density (**f**), and temperature (**g**) for the SolO (orange) and WIND (green) observations (1st event). The values of correlation coefficients in the figure are similar to Figure 2a. Correlation coefficients after correction of the time shift for each subinterval are presented in Table 1.

The IMF magnitude and components turned out to be the most unstable parameters, with high fluctuation levels and with minimal correlation coefficients despite the fact that the spacecraft were quite close to each other. Figure 5a illustrates the time series of IMF magnitude with an overall correlation coefficient of 0.31 and correlation coefficients of 0.26, 0.34, and 0.42 for each of the three subintervals, respectively. The maximum correlation coefficient was observed for the radial component of IMF (0.54), but it was also quite low on the 2nd and 3rd subintervals. Overall, the lowest differences in the time series of all parameters were typically observed for the FAST stream.

The same trends were typical for the time series considered separately on each subinterval. The time shift determined by means of the correlation analysis (see Section 2.3) could be rather different from the original one, up to several hours for a large separation of the spacecraft. For the 1st event, when the separation between the spacecraft was 0.1 AU, the time shifts after correction were 9:12, 9:06, and 9:09 for the three considered subintervals. Thus, there were no significant differences between the time shifts for subintervals; however, the shift differed by 2 h from the preliminary estimation based on the spacecraft separation and the SW speed. The values of correlation coefficients for all discussed parameters after time shift clarification are shown in Table 1.

Meanwhile, the correlation coefficient varied significantly from one subinterval to another due to observations of different types of SW. For example, Figure 6 shows the correlation coefficients between the bulk speed on the pair of spacecraft during subinterval 3. The correlation coefficient reached as low as -0.27 for the HCS, while they were 0.88 and 0.59 for the slow, quasi-stationary SW before and after the HCS crossing.
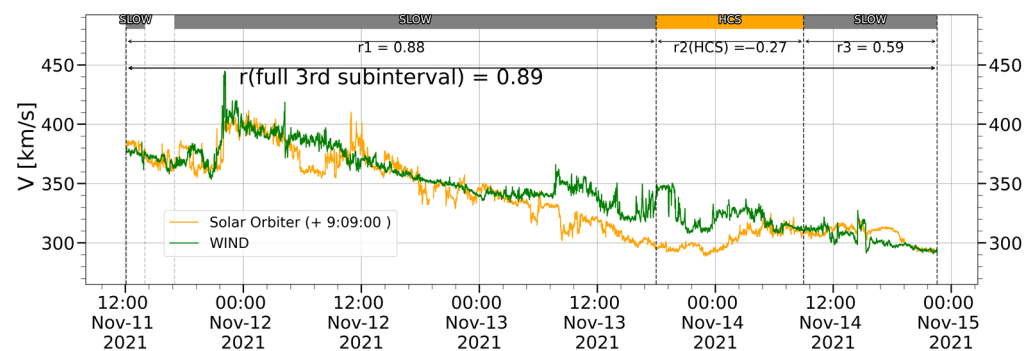

Figure 6. Comparison of bulk speed time series for the third subinterval (1st event), taking into account the time shift after correction. The color bar at the top of the chart shows the periods of different large-scale SW structures. Correlation coefficients for the full 3rd subinterval (r) and for different SW structures (r1, r2, r3) are shown on the chart.

When spacecraft are close to each other, the absolute values of the parameters usually do not change significantly; however, it does not always indicate a high correlation coefficient. After correction of the time shift of the 1st subinterval, the correlation coefficient of the radial component of IMF reaches 0.52. The correlation coefficients are 0.55 and 0.23 for tangential and normal components, respectively (see Figure 7). Differences and similarities in the time series of IMF parameters, when observed at small distances between the spacecraft, are often related to observed structures in the distinct SW type. For example, for the radial IMF component, there is a structure within the FAST stream on 7 November which is visible on WIND and not visible on SolO, and the correlation is reduced (Figure 7a). In the following SLOW stream, the visual similarity is much higher.
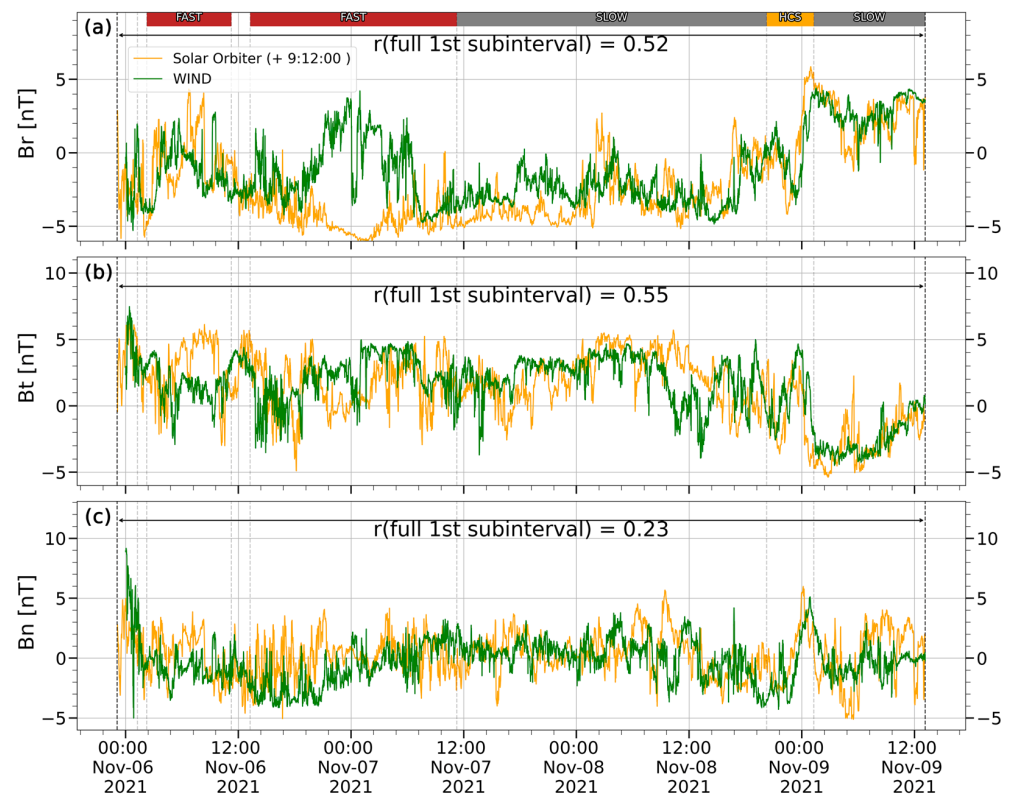
Figure 7. Comparison of time series of IMF components for the first subinterval (1st event). (**a**) Radial; (**b**) tangential; (**c**) normal. Correlation coefficients after correction of the time shift are indicated.

The comparison of simultaneous observations from two distant spacecraft (0.5 AU) provides a broader picture of the dynamics of the SW. Using the initial time-shift estimate (2 days, 3 h, and 5 min) in Equation (2), one of the highest values of the correlation coefficients, 0.68, was observed for the bulk speed value, similar to the first interval (see Figure 8e). The second interval was also divided into three subintervals in accordance with the prominent plasma structures: abrupt increase and smooth decrease in the bulk speed in the first, oscillations in the second, and sudden enhancements after a stable flow in the third. For the first subinterval (2 March 2022 21:05:00 UT–7 March 2022 22:59:51 UT), the correlation coefficient of the bulk speed was equal to 0.88, while for the second (7 March 2022 22:59:51–9 March 2022 08:59:51 UT) and third (9 March 2022 08:59:51 UT–12 March 2022 07:11:00 UT), it dropped significantly to 0.28 and −0.01, respectively. Here, corrections to the time shift played crucial role. At the same time, the average bulk speed value remained almost unchanged. Similar trends could be seen for the correlation coefficient of the temperature time series (see Figure 5g), but its absolute value decreased several times over the propagation time. The IMF magnitude also significantly decreased with increasing distance (which is quite natural), but its correlation remained relatively high. The intervals containing SHEATH, EJECTA, and MC were characterized by higher IMF magnitude correlation than those containing FAST and HCS. The time series of SLOW streams matched well, but the correlation was worse, while the worst match was observed in the CIR stream. For the 2nd interval, the lowest correlation value among the IMF components was obtained for the radial component (Figure 8b), which was opposite to the results for the 1st interval. The measurements of proton density illustrated in Figure 8f demonstrated the worst similarity among the parameters under study. This result was also relevant for the 1st interval. The time series could undergo significant distortions at analyzed distances, but some prominent structures could persist for quite a long time. For example, Figure 8e shows that a rapid increase in the bulk speed from ~300 to 650 km/s for the SolO and up to 550 km/s for WIND was observed on both spacecraft, although the

arrival times and the individual details of the bulk speed time series after the interplanetary shock were different. The application of the corrected estimate (see Section 2.4) for the third subinterval contributed to a significant increase in the correlation coefficient for almost all parameters (see Table 1).
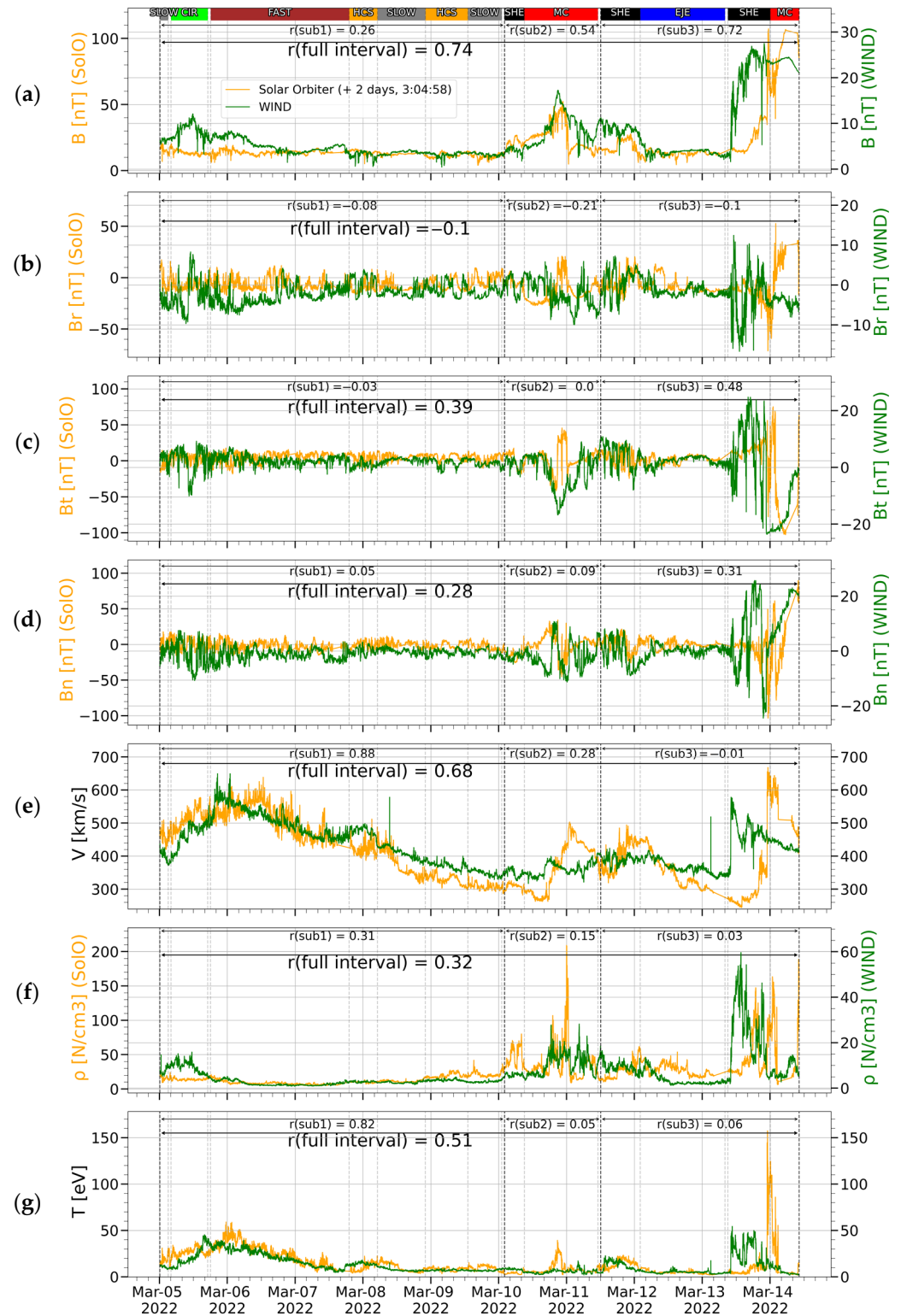

Figure 8. Comparison of the time series of the IMF magnitude (**a**) and IMF components in RTN system (**b**–**d**), bulk speed (**e**), proton density (**f**), and temperature (**g**) for SolO and WIND (2nd event). All signatures are the same as in Figure 2.

3.2. Histogram Analysis

First, we studied the distributions over the whole intervals. As shown in Section 3.1, the IMF magnitude and proton density demonstrated high variability when comparing data from two spacecraft, even at relatively small distances (~0.1 AU). The full set of distributions for all considered parameters is presented in Figure 9. All distributions had fairly broad shapes. A statistical comparison showed that the distributions of IMF magnitude (Figure 9a), bulk speed (Figure 9c), and proton temperature (Figure 9d) changed slightly as the SW plasma propagated between the spacecraft (within 12% for magnetic field and temperature and within 3% for the bulk speed). On the other hand, a significant discrepancy in the shape and basic characteristics of proton density (Figure 9b) distributions (median values differed by ~30%) was observed. At the same time, the STD, SEM, and the Norm STD, reflecting the fluctuation level during the interval, varied slightly for all quantities. All of the above statistical characteristics are presented in Table 2.
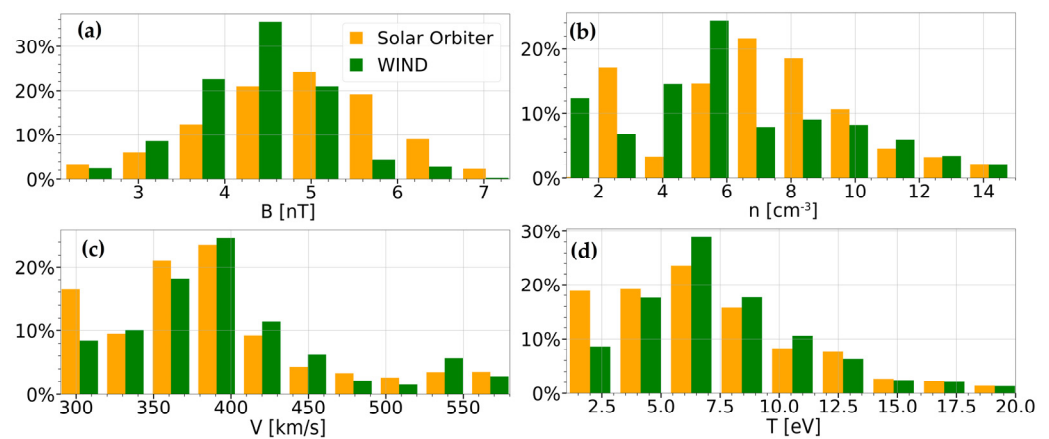

Figure 9. Comparison of distribution histograms (1st event). (**a**) IMF magnitude; (**b**) SW proton density; (**c**) SW bulk speed; (**d**) SW proton temperature.

Table 2. Comparison of statistical parameters for IMF magnitude (B), SW proton density (n), SW bulk speed (V), and SW proton temperature (T) for the 1st event (columns 2 and 3) and for the 2nd event (columns 4 and 5) on SolO (column 2 and 4) and WIND (column 3 and 5) measurements, respectively.

	SolO (1st Event)	WIND (1st Event)	SolO (2nd Event)	WIND (2nd Event)
Mean B (nT)	4.8 ± 0.01	4.3 ± 0.01	19.6 ± 0.04	6.6 ± 0.01
Median B (nT)	4.9	4.3	14	4.7
STD B (nT)	1.1	1	18	5.1
Norm STD B (%)	23.5	22.1	91.8	77.1
Mean V (km/s)	394.2 ± 0.17	404.9 ± 0.18	404.8 ± 0.21	420.8 ± 0.15
Median V (km/s)	380.9	388.8	407	403.3
STD V (km/s)	75.5	77.7	93.2	65.7
Norm STD V (%)	19.2	19.2	23	15.6
Mean n (cm^{-3})	7.5 ± 0.01	6.2 ± 0.01	22.7 ± 0.04	6.3 ± 0.02
Median n (cm^{-3})	7.2	5.5	17.3	3.5
STD n (cm^{-3})	3.7	3.4	19.9	7.1
Norm STD n (%)	49.6	54.4	87.8	112.3
Mean T (eV)	7 ± 0.01	7.4 ± 0.01	13.8 ± 0.03	12.5 ± 0.02
Median T (eV)	6.2	6.6	9.1	8.5
STD T (eV)	4.1	3.6	13.2	9.3
Norm STD T (%)	59.3	49.1	95.5	74.7

The difference observed in the distributions (especially for density, as the most variable parameter) may be explained by the fact that the distributions are common to all observed large-scale structures. Thus, one needs to consider the distributions for different SW types separately. An examination of the parameters' distributions for distinct SW types demonstrates remarkable features. For example, the density distribution for the CIR (see Figure 10a) on the SolO had a complex shape with three peaks: the first subset of plasma, with a density of ~7.5 cm^{-3}; the second subset, characterized by a density of ~9.5 cm^{-3}; and the third one, characterized by a density of ~13.5 cm^{-3}. However, when the SW reached WIND, two peaks with maxima at ~9 cm^{-3} and ~12.5 cm^{-3} could be observed instead of three peaks, as observed on the SolO. Perhaps two strongly interacting streams merged into one during the propagation. Note that WIND was, at this moment, at a radial distance of about 0.1 AU from SolO, at the same time that the distance between spacecraft in the plane perpendicular to the Sun–Earth line was ~10^6 km. Thus, the difference could also have been related to inhomogeneities of plasma structures in space, as we could see different parts of structures at different spacecraft.
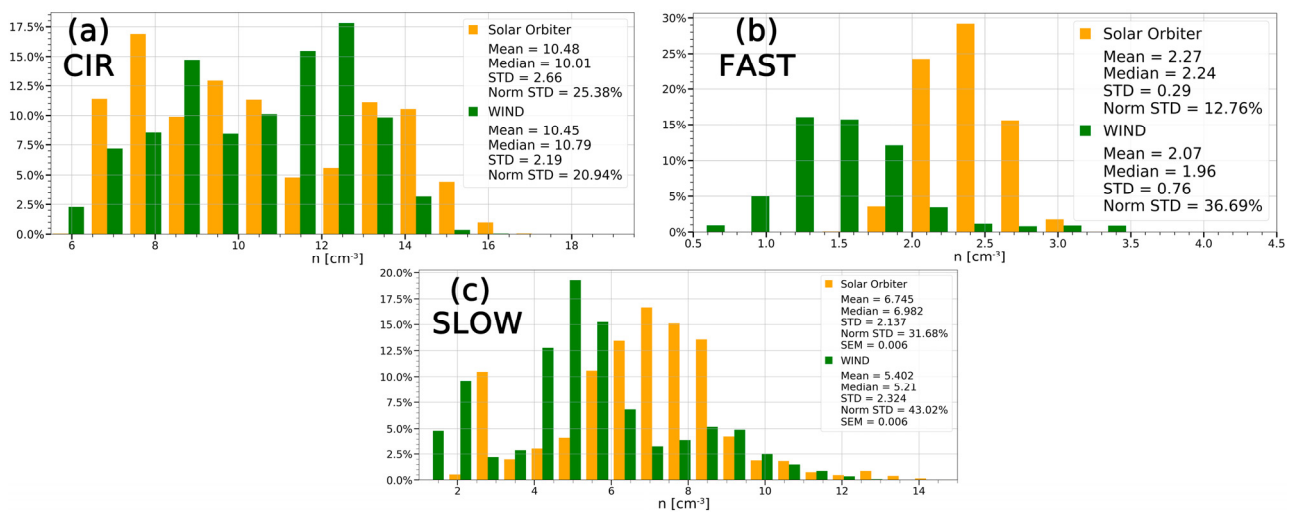

Figure 10. Density distributions in CIR (**a**), FAST (**b**), and slow SW (**c**) (1st event).

However, it should be noted that no other statistical characteristics of the distributions changed significantly, like in case of density distributions, over the entire 1st event.

The density distribution in the FAST stream also behaved differently at the two spacecraft (see Figure 10b). Note that this type involves a wide range of density values, including extremely high ones (not shown on histogram) compared to the average in the entire interval. Thus, to determine the mean and median values, the sample was limited to the range of the distribution in the figure. Two noticeably distinguished maxima could be observed for density distributions on different spacecraft. The main distribution mode had a peak at 2.4 cm^{-3} for SolO, which shifted to 1.3 cm^{-3} when plasma approached the WIND spacecraft.

Figure 10c presents the density distributions for slow SW streams, which also had different shapes for SolO and WIND measurements and differed from the distributions for CIR and FAST. These distributions also had complex shapes, with several peaks, which suggests that not only large-scale structures can determine the shapes of distributions, but their medium-scale substructures can as well.

Thus, the statistical distributions for density could be substantially modified even during the plasma motion time of ~9 h at a distance of 0.1 AU, and these changes may be different in various types of the SW streams. This feature is specific to the proton density; such noticeable differences in statistical distributions are not observed for other considered parameters.

For the second event (0.5 AU between the spacecraft), the histograms of the distributions differed significantly depending on the parameter (see Figure 11 and Table 2). The distributions for the proton temperature were the most similar, even though the measurements on the SolO had large scatter and reached 150 eV (extreme values were rare and are not shown in the Figure 11d). The bimodal bulk speed distribution (Figure 11c) registered at the SolO became more uniform at WIND. These differences may have also been due to the specifics of the measurements in different positions—some plasma structures observed on one spacecraft were not observed on another. The values of all statistical parameters remained approximately the same for the bulk speed and proton temperature. The histograms for the IMF magnitude (Figure 11a) showed clear similarity in their shapes, but with significantly shifted absolute values of the distribution maximum (mean and median values, respectively), which were consistent with the decrease in the IMF magnitude with the distance from the Sun. However, the Norm STD of IMF magnitude differed by only 20%. Density distributions (Figure 11b) still showed the greatest differences in both shape and all statistical parameters (see Table 2, column 4 and 5). Despite the differences in distributions, Norm STD differed by only 25% on average. STD for density increased when the SW approached the Earth, while the Norm STD for other parameters decreased by 10–20%. Thus, an increase in the level of density fluctuations was observed.
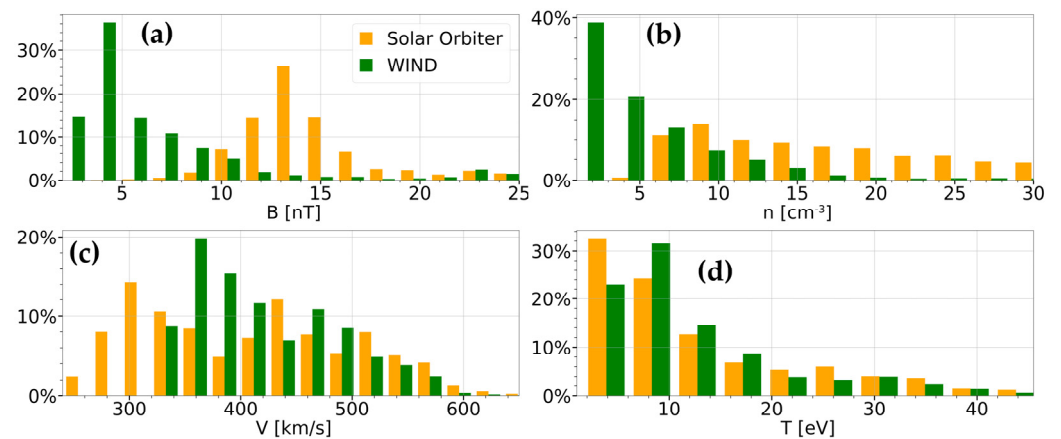

Figure 11. Comparison of distribution histograms (2nd event). (**a**) IMF magnitude; (**b**) proton density; (**c**) bulk speed; (**d**) proton temperature.

In the case of proton density and the IMF magnitude, it is quite natural to observe significant differences in mean values in accordance with solar wind propagation models. But it is surprising that the values of Norm STD, characterizing the relative level of fluctuations, changed weakly for almost all observed parameters. Note that, based on the value of the Norm STD, the level of fluctuations decreased slightly for all parameters except proton density, when SW moved to the Earth's orbit. The relative level of density fluctuations, on the contrary, increased.

Considering the differences in statistical distributions for individual types of SW, as was produced for the first interval, a number of peculiarities can be highlighted for the second event. For example, the IMF magnitude distribution in CIR streams (see Figure 12a) on SolO had a single large peak on the background of a broad and flat distribution, while on WIND, two closely located peaks were observed. However, the mean and median values differed less than for the same distributions of SW as a whole (Figure 11a). At the same time, the other statistical parameters (the basic and Norm STD) were similar for these two distributions and had relatively small values.
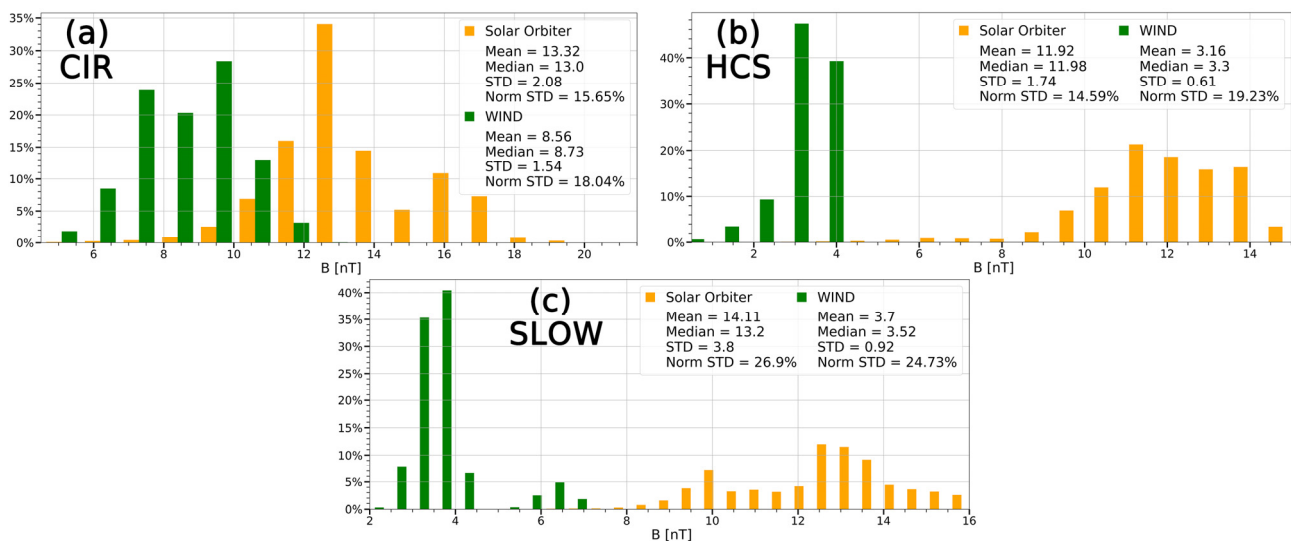
Figure 12. IMF magnitude distributions in CIR (**a**), HCS (**b**), and slow SW (**c**) (2nd event).

As the SW moves away from the Sun, it undergoes various interactions with the surrounding space, which may affect its characteristics. This effect may be more pronounced for some types of SW. For example, distributions of IMF magnitude in HCS (see Figure 12b) undergo significant changes in shape as well as in the most probable values. However, the Norm STD and STD parameters stay nearly unchanged.

The distributions in the slow SW (see Figure 12c) demonstrate a complex picture with two peaks (reflecting two plasma subsets). While the mutual position of the peaks stays the same at two distances from the Sun, the intensity of each peak changes—for SolO, the main peak is positioned at 13 nT and the less pronounced peak is positioned at 10 nT, and for WIND, oppositely, the main peak has the lower value of ~3.5 nT and the less pronounced peak has the higher value of ~6.5 nT.

The analysis of the histograms for all types of SW shows that the greatest changes occur in the SLOW, HCS, and ICME (MC) streams. However, these conclusions are preliminary, since a relatively small amount of statistical data have been collected so far for different SW types.

3.3. Fluctuation Analysis

Analysis of the fluctuation level and its dynamics is an important step in the study of the evolution of SW structures. As is shown above, a noticeable change in the absolute value of proton density may occur even at a small distance between the spacecraft (0.1 AU). Nevertheless, the levels of fluctuations (RSD values) and their time series are preserved at both selected events, and the observed changes are usually related to the type of SW stream. For example, Figure 13 shows the time series of the Loc STD (see the Section 2 for definition) of proton density for the first interval. One can see that, in general, the levels of fluctuations were similar on both spacecraft (with a difference of ~25% on average), although the level of fluctuations varied intensively during each interval (changes in the fluctuation level could exceed 500% for each spacecraft).
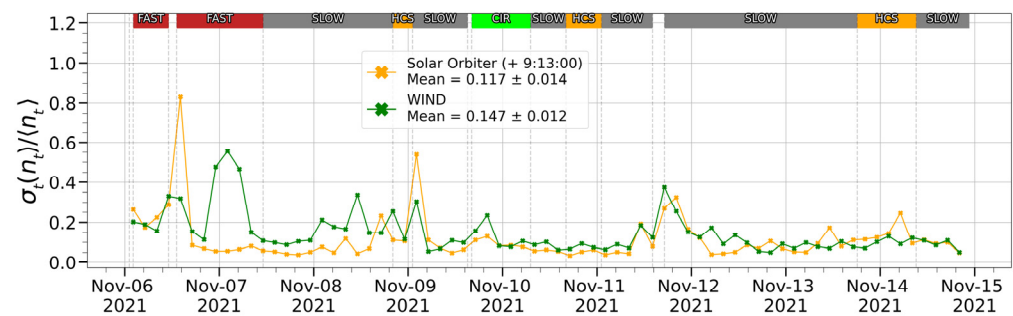
Figure 13. Time evolution of the fluctuation level for proton density (1st event).

At the same time, in some of the large-scale structures (FAST, HCS, and CIR), simultaneous increases in the levels of fluctuations and the amplitudes of these increases were also similar (with differences of ~25%). However, for the FAST stream on 7 November, in contrast, a significant difference was observed—the large peak of Loc STD for density could be seen on WIND data at 7 November 2021~04:00; however, it was not observed by SolO. This difference was caused by the density structure, which was observed by WIND and not by SolO (see Figure 5).

The results were similar for a large distance between the spacecraft (0.5 AU). As shown above, significant changes in the absolute values of the parameters are possible, especially for IMF magnitude and proton density, with increasing distance. Nevertheless, weak changes in local levels of fluctuations were observed for all of the studied SW parameters. In particular, the time series of the Loc STD were similar and almost matched for some periods for both spacecraft distances (with a difference of 8% on average). It was significantly less than the difference in the level of fluctuations for a single spacecraft, which exceeded 1000%. The difference between fluctuation level at two points stayed within 8% even for proton density, which was the most variable parameter (see Figure 14). The time moments when the difference of the Loc STD was pronounced were usually associated with some local structures observed by one of the spacecraft and not observed by another, or modified substantially during the propagation. For example, in the vicinity of the MC and IS, the greatest Loc STD differences occurred up to 450%, which is still less than the difference in the fluctuation level on each spacecraft.
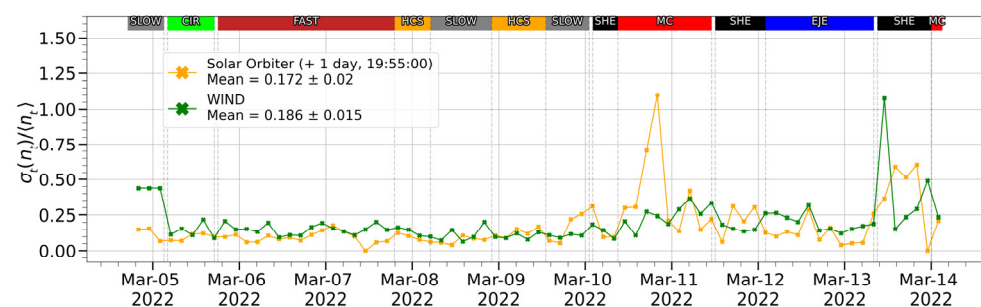

Figure 14. Time evolution of the fluctuation level for proton density (2nd event).

We provide a detailed comparison of density as the parameter with the maximum level of fluctuations. For other parameters, similar results were obtained.

This result is consistent with the fluctuations' evolution for the first event. In both cases, certain types of SW significantly increased the overall difference in mean values. For this reason, we can conclude that the level of local fluctuations changes slightly when the wind moves from the Sun to Earth. However, it can vary for different SW types (according to simultaneous observations on two spacecraft), as well as for some local structures (observed by one of the spacecraft). Such local structures can be found even in cases where there is a small distance between the spacecraft, so it is a result of the spatial inhomogeneity of the SW rather than evolution during the propagation.

3.4. Analysis of the 4th-Order Moment of the PDF

In addition to the quite high coincidence of the amplitude and time series of the fluctuations of the SW parameters on different spacecraft, we can note that the high-order statistical properties of PDFs of the fluctuations for each parameter were also similar. In this study, we analyze the fluctuations of IMF magnitude, proton density, and bulk speed. Figure 15 shows that the dependences of the flatness (4th-order moment of the PDF) vs. the time scale for the spacecraft separation of 0.1 AU had similar properties on SolO and WIND for all observed SW parameters. Overall, there was a decrease in the flatness with the increase in scale, and the flatness tended to approach 3 at scales above 10^4 s, indicating the presence of intermittency in the discussed flows (see Section 2.7). The same trends were observed for other two subintervals of the 1st event.
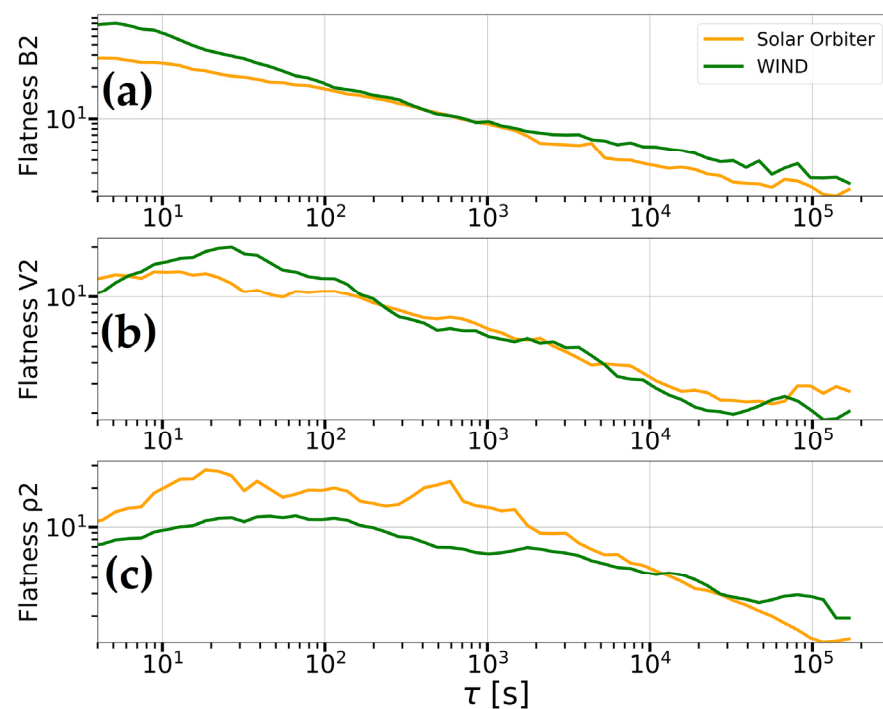

Figure 15. Comparison of the flatness dependence on the scale for the second subinterval of the 1st event. (**a**) IMF magnitude; (**b**) bulk speed; (**c**) proton density.

Nevertheless, we can note some differences in the behavior of the above-described dependences for different SW parameters. For example, the PDF of IMF fluctuations tended to become Gaussian distribution more smoothly than for other parameters (see, for example, Figure 15a for the second subinterval of the first interval). For density fluctuations, there were some differences in the flatness values at all scales, which was natural for such a variable parameter. However, the trend of decreasing flatness with increasing scale still persisted for measurements on both spacecraft.

The tendency of flatness vs. scale dependence for parameter fluctuations was similar in the second event, with significant separation between the spacecraft of ~0.5 AU (see, for example, Figure 16 for the second subinterval of the second event). However, there were some features of statistical properties of fluctuations in different parameters.
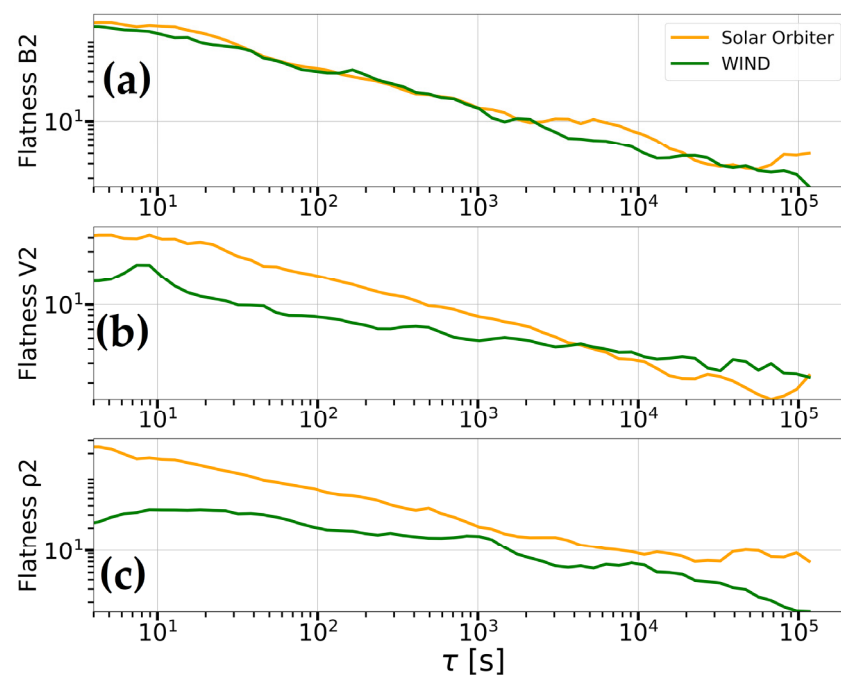
Figure 16. Comparison of the flatness dependence on the scale for the second subinterval of the 2nd event. (**a**) IMF magnitude; (**b**) bulk speed; (**c**) proton density.

For IMF magnitude fluctuations (Figure 16a), there was a nearly exact match of flatness dependence at two spacecraft, while for bulk speed (Figure 16b) and density (Figure 16c) fluctuations, there were discrepancies in the flatness profiles. The largest discrepancy was observed for the proton density fluctuations—the flatness value in general was less at the WIND spacecraft (Figure 16c). This means that the distribution tails became lighter and large-amplitude fluctuations became less frequent for the WIND density measurements.

This fact may indicate a decrease in the level of intermittency during plasma propagation to Earth. However, such a tendency was not observed for all intervals; there were also examples of inverse situations. Note that the flatness, calculated on several subintervals, showed a large scatter and requires a more detailed analysis.

Thus, as discussed above, and as can be seen from Figures 15 and 16, the flatness can vary significantly for different SW parameters and from one time interval to another for the same parameter. But in general, similar patterns of flatness versus the time scale were observed for most of the subintervals. We can conclude that the characteristics of intermittency, one of the features of the turbulent SW flow, generally changed weakly with distance for most of the parameters. Nevertheless, for some parameters in several subintervals, these differences can be significant, which requires more detailed study.

4. Discussion

In this study, we have addressed how the characteristics of fluctuations change as plasma propagates in the heliosphere from one point located half the distance from the Sun to Earth to another point close to Earth. We investigated two long intervals of simultaneous observations on the SolO and WIND spacecraft, located at distances of 0.1 and 0.5 AU from each other. The dynamics of the SW structures were analyzed at a wide range of scales due to the use of long data series with high temporal resolution. A peculiarity of this comparison is the possibility to trace properties of fluctuations embedded in the different SW structures, which typically have different bulk speeds. The good correspondence of observations on two closely located spacecraft in the 1st event indicated appropriate data selection and correction methods (see Section 2.4), which allowed us to compare the observations at significant distances between the spacecraft.

We used the correlation analysis method described in [36] to find the optimal time shift and compare the SW parameters, which allowed us to increase the correlation of large-scale structures and trace them on their way between the spacecraft. In addition, we were able to examine the effects of different types of SW on the correlation coefficient and identify the most variable and stable physical quantities and SW stream phenomena. The bulk speed was the most unchanging parameter, while the proton density and magnetic field parameters exhibited the highest variability.

In [19], the use of multipoint measurements from five spacecraft helped to broadly describe 17 CME phenomena, to find their complex structures with several components, and to show different behavior depending on the distance from the Sun. Our research was focused on the study of similar sets of SW and IMF parameters with the help of data from only two spacecraft. Measurements were made near the Sun–Earth line, but at different distances from the Sun, which allowed us to detect and study the evolution of fluctuations and the differences in several CIRs and ICME (MC) streams near the Sun–Earth line which may be geoeffective.

Our study included not only a comparison of time series, but also an analysis of the statistical properties. In particular, we analyzed histograms of the SW parameters in general and in different stream types with a wide range of statistical parameters. Note that, if the changes of the absolute values of proton density and magnetic field magnitude looked quite natural, the similarity of the Norm STD (which roughly reflect the level of fluctuations) at two distances from the Sun was surprising.

The most complex parameter distributions and largest changes were observed for the SLOW, HCS, and ICME(MC) SW types. The complex distribution shape could be related to the presence of a set of substructures within the large-scale structures. On the other hand, similar distributions are often observed in the SW, which may be the result of the presence of different plasma populations [37]. In this study, we have demonstrated only a small fraction of the collected statistics for different types of SW, focusing on two parameters. More detailed studies are planned that will expand our understanding of the statistical properties of the various streams and their dynamics in the heliosphere.

An important part of this work was devoted to the consideration of fluctuation properties in the SW streams. The analysis of the Loc STD at three-hour subintervals using multipoint comparisons of the parameters made it possible to understand the dynamics of the fluctuation levels and the influence of different SW types on this process. The average local power of fluctuations varies slightly regardless of the distance, but it can vary significantly for different SW types. At the same time, a great difference in the local fluctuation levels at two points can indicate that some plasma structures have been observed by only one of the spacecraft. Moreover, such a difference may occur even for a small distance between the observation points along the Sun–Earth line. This cannot be explained by the SW evolution during the propagation, and is most likely to be the signature of the SW flow's inhomogeneity in the direction perpendicular to the Sun–Earth line, that is, the limited size of the structure in this plane.

In the last part of the fluctuation analysis, we investigated SW inhomogeneity considering the properties of the PDFs of fluctuations at different time scales. We used an approach similar to [21,39]. Bruno and Carbone [21] found a difference in the dynamics of the intermittency of bulk speed and IMF components between FAST and SLOW streams within long observation intervals, where only FAST wind intermittency increased with the radial distance. The growth of intermittency with distance from the Sun is also shown in [22], with the help of Ulysses and ACE data. At the current stage of the study, we have considered the flatness value at various scales through measurements of both spacecraft. The situations for different parameters and for different intervals can be completely varied, but in general, the most important fact is that the trend of flatness increasing from large to small scales could be observed for all considered parameters and for all discussed intervals. But we did not find any significant differences in the intermittency properties of the SolO or the WIND, regardless of the distance between them. This result is valid even for proton

density (the most variable parameter). Some cases exhibited increases in intermittency when approaching Earth. However, a more detailed analysis is required in order to draw accurate conclusions regarding the evolution of intermittency over long distances.

5. Conclusions

The main results of this research can be summarized as follows:

1. On average, high correlation between the time series of the SW plasma and IMF parameters was observed at distances of both 0.1 and 0.5 AU (the average value of the correlation coefficient exceeded 0.5);
2. The bulk speed underwent the smallest changes (average correlation coefficient was about 0.8), and the IMF magnitude and proton density were the most variable parameters;
3. The correlation coefficient may significantly vary for different large-scale types of SW;
4. Mainly, the relative fluctuations stayed unchanged at distances over 0.1 and 0.5 AU for all parameters, regardless of the changes in their absolute amplitudes;
5. Local fluctuation levels varied slightly with distance and may change in different types of SW streams or in some plasma structures;
6. The characteristics of fluctuations of the same plasma volume observed at different distances from the Sun differed much less than those observed on one spacecraft but for different time intervals;
7. The tendency of growth of PDFs' non-Gaussianity to smaller scales was preserved over different distances, which may indicate that the level of intermittency also stays unchanged when the SW streams propagate to the Earth's orbit.

The presented study shows that the characteristics of fluctuations (including the level of intermittency) change slightly with distance, while differences in absolute parameters values are observed as expected in accordance with the solar wind models. The study of the properties of SW at different distances from the Sun to the Earth can help to enhance the capability of the space weather predictions, specifically by developing advanced techniques for tracing the interplanetary phenomena and their impacts on Earth.

Author Contributions: Conceptualization, M.O.R. and Y.I.Y.; methodology, I.D.V., M.O.R. and L.S.R.; software, I.D.V.; validation, M.O.R. and L.S.R.; investigation, I.D.V.; writing—original draft preparation, I.D.V. and M.O.R.; writing—review and editing, I.D.V. and M.O.R.; visualization, I.D.V. and A.A.K.; supervision, Y.I.Y. All authors have read and agreed to the published version of the manuscript.

Conflicts of Interest: The authors declare no conflicts of interest.

References

1. Marsch, E. Solar Wind Models from the Sun to 1 AU: Constraints by in Situ and Remote Sensing Measurements. *Space Sci. Rev.* **1999**, *87*, 1–24. [CrossRef]
2. Verscharen, D.; Klein, K.G.; Maruca, B.A. The multi-scale nature of the solar wind. *Living Rev. Sol. Phys.* **2019**, *16*, 5. [CrossRef] [PubMed]
3. Petrukovich, A.A.; Malova, H.V.; Popov, V.Y.; Maiewski, E.V.; Izmodenov, V.V.; Katushkina, O.A.; Vinogradov, A.A.; Riazantseva, M.; Rakhmanova, L.S.; Podladchikova, T.V.; et al. Modern view of the solar wind from micro to macro scales. *Phys. Uspekhi* **2020**, *63*, 801–811. [CrossRef]
4. Feldman, W.C.; Asbrige, J.R.; Bame, S.J.; Gosling, J.T. Longterm variations of selected solar wind properties: IMP 6, 7 and 8 results. *J. Geophys. Res. Space Phys.* **1978**, *83*, 2177–2189. [CrossRef]

5.   Schwenn, R. Solar Wind Sources and Their Variations over the Solar Cycle. In *Solar Dynamics and Its Effects on the Heliosphere and Earth*; Baker, D.N., Klecker, B., Schwartz, S.J., Schwenn, R., Von Steiger, R., Eds.; Space Sciences Series of ISSI; Springer: New York, NY, USA, 2007; Volume 22, pp. 51–76. [CrossRef]

6.   Yermolaev, Y.I.; Nikolaeva, N.S.; Lodkina, I.G.; Yermolaev, M.Y. Catalog of Large-Scale Solar Wind Phenomena during 1976–2000. *Cosm. Res.* **2009**, *47*, 81–94. [CrossRef]

7.   Kilpua, E.K.J.; Balogh, A.; Von Steiger, R.; Liu, Y.D. Geoeffective Properties of Solar Transients and Stream Interaction Regions. *Space Sci. Rev.* **2017**, *212*, 1271–1314. [CrossRef]

8.   Marsch, E. MHD Turbulence in the Solar Wind. In *Physics of the Inner Heliosphere II. Particles, Waves and Turbulence*; Schwenn, R., Marsch, E., Eds.; Physics and Chemistry in Space; Springer: Berlin/Heidelberg, Germany, 1991; Volume 21, pp. 159–241. [CrossRef]

9.   Bavassano, B. The solar wind: A turbulent magnetohydrodynamic medium. *Space Sci. Rev.* **1996**, *78*, 29–32. [CrossRef]

10. Tsurutani, B.T.; Ho, C.M. A review of discontinuities and Alfvén waves in interplanetary space: Ulysses results. *Rev. Geophys.* **1999**, *37*, 517–541. [CrossRef]

11. Borovsky, J.E. On the flux-tube texture of the solar wind: Strands of the magnetic carpet at 1 AU? *J. Geophys. Res. Space Phys.* **2008**, *113*, A08110. [CrossRef]

12. Hudson, P.D. Discontinuities in an anisotropic plasma and their identification in the solar wind. *Planet. Space Sci.* **1970**, *18*, 1611–1622. [CrossRef]

13. Taylor, G.I. The Spectrum of Turbulence. *Proc. R. Soc. Lond. Ser. Math. Phys. Sci.* **1997**, *164*, 476–490. [CrossRef]

14. Burlaga, L.; Sittler, E.; Mariani, F.; Schwenn, R. Magnetic loop behind an interplanetary shock: Voyager, Helios, and IMP 8 observations. *J. Geophys. Res.* **1981**, *86*, 6673–6684. [CrossRef]

15. Prise, A.J.; Harra, L.K.; Matthews, S.A.; Arridge, C.S.; Achilleos, N. Analysis of a coronal mass ejection and corotating interaction region as they travel from the Sun passing Venus, Earth, Mars, and Saturn. *J. Geophys. Res. Space Phys.* **2015**, *120*, 1566–1588. [CrossRef]

16. Lugaz, N.; Winslow, R.M.; Farrugia, C.J. Evolution of a long-duration coronal mass ejection and its sheath region between Mercury and Earth on 9–14 July 2013. *J. Geophys. Res. Space Phys.* **2020**, *125*, e2019JA027213. [CrossRef]

17. Good, S.W.; Kilpua, E.K.J.; LaMoury, A.T.; Forsyth, R.J.; Eastwood, J.P.; Möstl, C. Self-similarity of ICME flux ropes: Observations by radially aligned spacecraft in the inner heliosphere. *J. Geophys. Res. Space Phys.* **2019**, *124*, 4960–4982. [CrossRef]

18. Möstl, C.; Farrugia, C.J.; Kilpua, E.K.J.; Jian, L.K.; Liu, Y.; Eastwood, J.P.; Harrison, R.A.; Webb, D.F.; Temmer, M.; Odstrcil, D.; et al. Multipoint shock and flux rope analysis of multiple interplanetary coronal mass ejections around 2010 August 1 in the inner heliosphere. *Astrophys. J.* **2012**, *758*, 18. [CrossRef]

19. Möstl, C.; Weiss, A.J.; Reiss, M.A.; Amerstorfer, T.; Bailey, R.L.; Hinterreiter, J.; Bauer, M.; Barnes, D.; Davies, J.A.; Harrison, R.A.; et al. Multipoint Interplanetary Coronal Mass Ejections Observed with Solar Orbiter, BepiColombo, Parker Solar Probe, Wind, and STEREO-A. *Astrophys. J. Lett.* **2022**, *924*, L6. [CrossRef]

20. Bruno, R.; Carbone, V. The Solar Wind as a Turbulence Laboratory. *Living Rev. Sol. Phys.* **2013**, *10*, 2. [CrossRef]

21. Bruno, R.; Carbone, V.; Sorriso-Valvo, L.; Bavassano, B. Radial evolution of solar wind intermittency in the inner heliosphere. *J. Geophys. Res.* **2003**, *108*, 1130. [CrossRef]

22. D'Amicis, R.; Bruno, R.; Pallocchia, G.; Bavassano, B.; Telloni, D.; Carbone, V.; Balogh, A. Radial Evolution of Solar Wind Turbulence during Earth and Ulysses Alignment of 2007 August. *Astrophys. J.* **2010**, *717*, 474–480. [CrossRef]

23. Bruno, R.; Trenchi, L. Radial Dependence of the Frequency Break between Fluid and Kinetic Scales in the Solar Wind Fluctuations. *Astrophys. J. Lett.* **2014**, *787*, L24. [CrossRef]

24. Telloni, D. Spacecraft radial alignments for investigations of the evolution of solar wind turbulence: A review. *J. Atmosph. Sol.Ter. Phys.* **2023**, *242*, 105999. [CrossRef]

25. Alberti, T.; Milillo, A.; Heyner Hadid, L.Z.; Auster, H.-H.; Richter, I.; Narita, Y. The "Singular" Behavior of the Solar Wind Scaling Features during Parker Solar Probe–BepiColombo Radial Alignment. *Astrophys. J.* **2022**, *926*, 174. [CrossRef]

26. Telloni, D.; Sorriso-Valvo, L.; Woodham, L.D.; Panasenco, O.; Velli, M.; Carbone, F.; Zank, G.P.; Bruno, R.; Perrone, D.; Nakanotani, M.; et al. Evolution of Solar Wind Turbulence from 0.1 to 1 au during the First Parker Solar Probe–Solar Orbiter Radial Alignment. *Astrophys. J. Lett.* **2021**, *912*, 8. [CrossRef]

27. Sioulas, N.; Velli, M.; Huang, Z.; Shi, C.; Bowen, T.A.; Chandran, B.D.G.; Liodis, I.; Davis, N.; Bale, S.D.; Horbury, T.S.; et al. On the Evolution of the Anisotropic Scaling of Magnetohydrodynamic Turbulence in the Inner Heliosphere. *Astrophys. J.* **2023**, *951*, 12. [CrossRef]

28. Lepping, R.P.; Acūna, M.H.; Burlaga, L.F.; Farrell, W.M.; Slavin, J.A.; Schatten, K.H.; Mariani, F.; Ness, N.F.; Neubauer, F.M.; Whang, Y.C.; et al. The Wind Magnetic Field Investigation. *Space Sci. Rev.* **1995**, *71*, 207–229. [CrossRef]

29. Lin, R.P.; Anderson, K.A.; Ashford, S.; Carlson, C.; Curtis, D.; Ergun, R.; Larson, D.; McFadden, J.; McCarthy, M.; Parks, G.K.; et al. A Three-Dimensional Plasma and Energetic Particle Investigation for the Wind Spacecraft. *Space Sci. Rev.* **1995**, *71*, 125–153. [CrossRef]

30. Ogilvie, K.W.; Chornay, D.J.; Fritzenreiter, R.J.; Hunsaker, F.; Keller, J.; Lobell, J.; Miller, G.; Scudder, J.D.; Sittler, E.C.; Torbert, R.B.; et al. SWE, a Comprehensive Plasma Instrument for the WIND Spacecraft. *Space Sci. Rev.* **1995**, *71*, 55–77. [CrossRef]

31. Horbury, T.S.; O'Brien, H.; Carrasco Blazquez, I.; Bendyk, M.; Brown, P.; Hudson, R.; Evans, V.; Oddy, T.M.; Carr, C.M.; Beek, T.J.; et al. The Solar Orbiter Magnetometer. *Astron. Astrophys.* **2020**, *642*, A9. [CrossRef]

32. Owen, C.J.; Bruno, R.; Livi, S.; Louarn, P.; Janabi, K.A.; Allegrini, F.; Amoros, C.; Baruah, R.; Barthe, A.; Berthomier, M.; et al. The Solar Orbiter Solar Wind Analyser (SWA) Suite. *Astron. Astrophys.* **2020**, *642*, A16. [CrossRef]
33. Yermolaev, Y.I.; Lodkina, I.G.; Yermolaev, M.Y. Dynamics of large-scale solar-wind streams obtained by the double superposed epoch analysis: 3. Deflection of the velocity vector. *Sol. Phys.* **2018**, *293*, 91. [CrossRef]
34. Thompson, W.T. Coordinate systems for solar image data. *Astron. Astrophys.* **2006**, *449*, 791–803. [CrossRef]
35. Weimer, D.; King, J. Improved Calculations of Interplanetary Magnetic Field Phase Front Angles and Propagation Time Delays. *J. Geophys. Res.* **2008**, *113*, A01105. [CrossRef]
36. Rakhmanova, L.; Riazantseva, M.; Zastenker, G. Correlation level between solar wind and magnetosheath plasma and magnetic field parameters. *Adv. Space Res.* **2016**, *58*, 157–165. [CrossRef]
37. Berčič, L.; Maksimović, M.; Landi, S.; Matteini, L. Scattering of Strahl Electrons in the Solar Wind between 0.3 and 1 Au: Helios Observations. *Mon. Not. R. Astron. Soc.* **2019**, *486*, 3404–3414. [CrossRef]
38. Riazantseva, M.O.; Budaev, V.P.; Rakhmanova, L.S.; Zastenker, G.N.; Šafránková, J.; Němeček, Z.; Přech, L. Comparison of Properties of Small-Scale Ion Flux Fluctuations in the Flank Magnetosheath and in the Solar Wind. *Adv. Space Res.* **2016**, *58*, 166–174. [CrossRef]
39. Sorriso-Valvo, L.; Carbone, V.; Veltri, P.; Consolini, G.; Bruno, R. Intermittency in the Solar Wind Turbulence through Probability Distribution Functions of Fluctuations. *Geophys. Res. Lett.* **1999**, *26*, 1801–1804. [CrossRef]